Electronic Supplementary Material (ESI) for Dalton Transactions.

Supplementary information: Synthesis and characterization of a new monometallic manganese layered double hydroxide

Damien Cornu,* Romain Coustel,
Guillaume Renaudin, Guillaume Rogez, Aurélien Renard, Pierrick Durand,
Cédric Carteret, Christian Ruby†

*damien.cornu@univ-lorraine.fr
†christian.ruby@univ-lorraine.fr

1 Colors of the solids

Figure S1: Color of the solution before (up left) and for various addition of $S_2O_8^{2-}$ (x = 0.12 (up right), 0.24 (down left) and 0.30 (down right)) in a R = 1.5 solution

2 pH measurement during synthesis

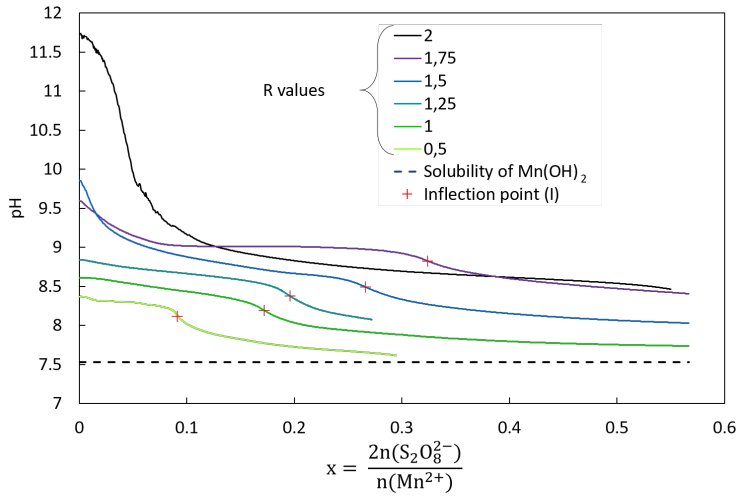

Figure S2: pH values for the Mn^{2+} solution after various NaOH addition characterized by various R values and during $S_2O_8{}^{2-}$ addition. Dotted line is the limit of the $Mn(OH)_2$ solubility with a Mn^{2+} concentration of 0.4 mol.L^{-1}. Red cross are the inflexion points reported on Figure S3.

Beside the characterization of the remaining ions in solution, another confirmation of the chemical reaction happening during $S_2O_8{}^{2-}$ addition is obtained by measuring the pH variation for various R values. Indeed, the initial quantity of $Mn_4(OH)_6SO_4$ is proportional to the R value.

On Figure S2, the variation of the pH against the x value is presented for various R between 0.5 and 2. For R = 2, $Mn(OH)_2$ is produced[1], the direct transformation of the pyrochroite into Mn_3O_4 is likely [2]. But for lower values, the variation of the pH against the x value presents an initial plateau. Let us define x_i the length of the plateau as the position of the inflection.

Figure S3 shows x_i against R. The inflexion of the pH curve occurs for x_i values proportional to tqhe R ratio and therefore to the quantities of $Mn_4(OH)_6SO_4$ in the solution. In the table S1, the theoretical inflexion values for the 4 equations described in the main text are gathered. The ratio observed on Figure S3 between the x_i and the R values confirms that the equation 2 (main text) is more likely. In addition, the pH drop from 9.8 to 8.5 for x from 0 to x_i (Figure 3) indicates that 6.10^{-5} mol.L^{-1} OH^- react during the reaction, which is a small change in the concentration compared to the initial concentration of Mn^{2+} that was equal to 0.23 mol.L^{-1}. The only equation that does not involve the consumption of OH^- is equation 2.

Equation	Product	Predicted x_i	pH change expected
1	$[Mn_6(OH)_{12}][SO_4{}^{2-}]$ (Mn-LDH)	0.33	Yes
2	$[Mn_6(OH)_{12}][SO_4{}^{2-}]$ (Mn-LDH)	0.25	No
3	Mn_3O_4	0.66	Yes
4	MnO(OH)	1	Yes

Table S1: Length of the initial plateau xi for various reactions according to their stoichiometry

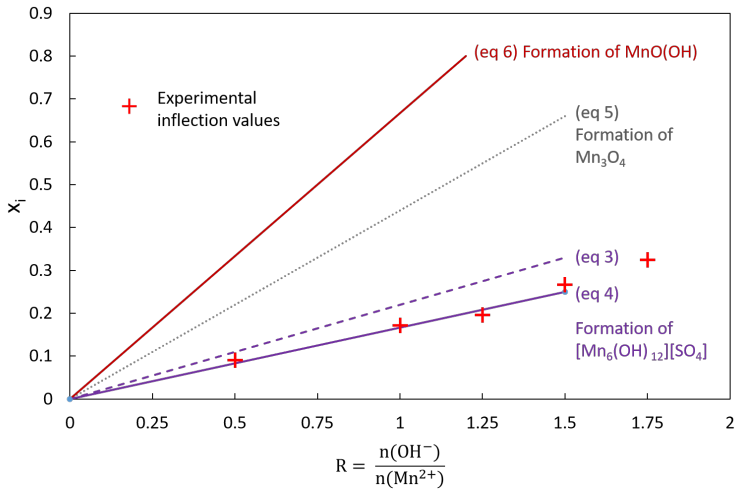

Figure S3: Position x_i of the inflection (maximum of the derivative of the pH curve from Figure S2) as a function of the ratio R

After the synthesis of LDH through equation 2, the oxidation of this LDH is explained by equation 5 (main text). Overall, the combination of the two steps can be described by the following equation:

$2\ Mn_4^{II}(OH)_6SO_4 + 2\ S_2O_8^{2-} \rightarrow 4Mn^{III}O(OH) + 4Mn^{2+} + 6SO_4^{2-} + 4H_2O$

3 Characterization of the Mn-LDH

3.1 X-ray Diffraction

The Le Bail matching is presented in figure S4 and in table S2.

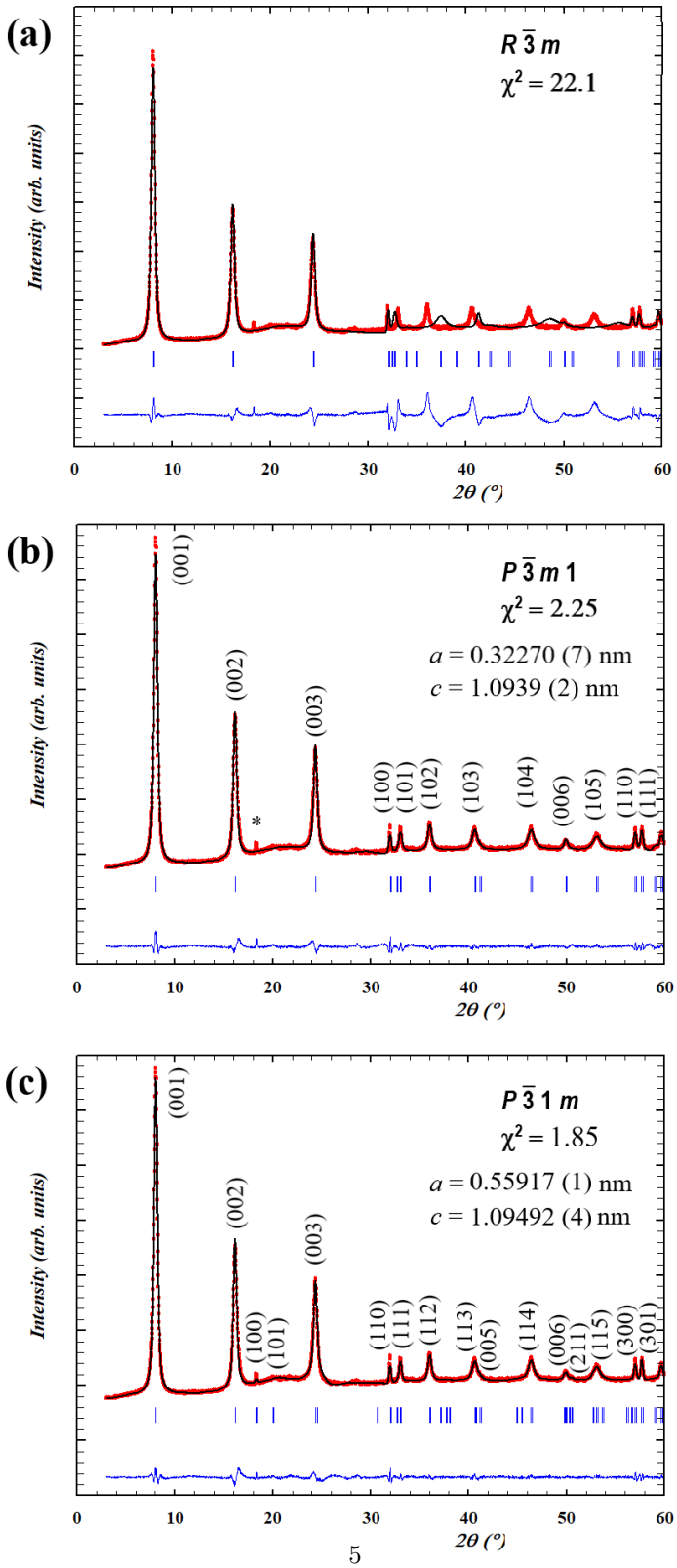

Figure S4: Le Bail matching for various space groups

Parameters	**Fe-LDH (SO_4^{2-})**	**Mn-LDH (SO_4^{2-})**
Space group	$P\bar{3}1m$	$P\bar{3}1m$
Lattice parameters (Å)		
a	5.5524 (1)	5.58821 (9)
c	11.011 (3)	10.9410 (4)
Atomic positions		
M^{3+} (1a)	(0 0 0)	(0 0 0)
M^{2+} (2c)	(2/3 1/3 0)	(2/3 1/3 0)
OH^- (6k)	(0.3250 0 0.0728(9))	(0.327(3) 0 0.0935(6))
H_2O (12l)	(-0.234(6) 0.619(3) 0.663(3))	(-0.248(3) 0.564(2) 0.6624(5))
S^{6+} (2e)	(0 0 0.641(5))	(0 0 0.6054(8))
$O_A{}^{2-}$ (2e)	(0 0 0.778(5))	(0 0 0.7481(7))
$O_B{}^{2-}$ (6k)	(0.256 0 0.596(5))	(0.275(2) 0 0.573(1))
Occupancies factors		
H_2O (12l)	0.35(3)	0.39(3)
$SO_4{}^{2-}$ (2e)	0.25(-)	0.25(-)
Reliability factors		
R_{Bragg}	0.11	0.031
R_{F}	0.071	0.060
R_{p}	0.061	0.027
R_{wp}	0.085	0.036
R_{exp}	0.094	0.026

Table S2: Comparison of the parameters for the Fe LDH and the Mn LDH

3.2 Scanning Electron Microscopy

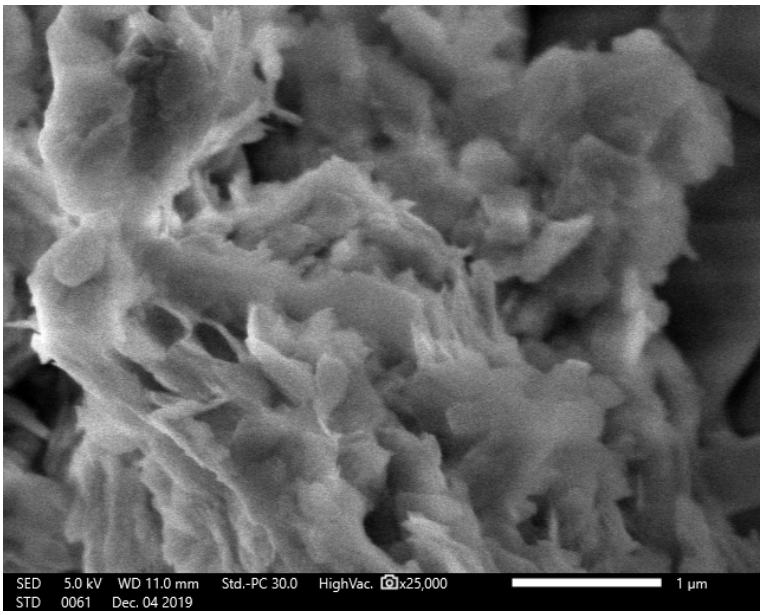

Figure S5: SEM picture of the R = 1.5 solid before oxidation. White bar is 1 μm

3.3 Infrared spectroscopy

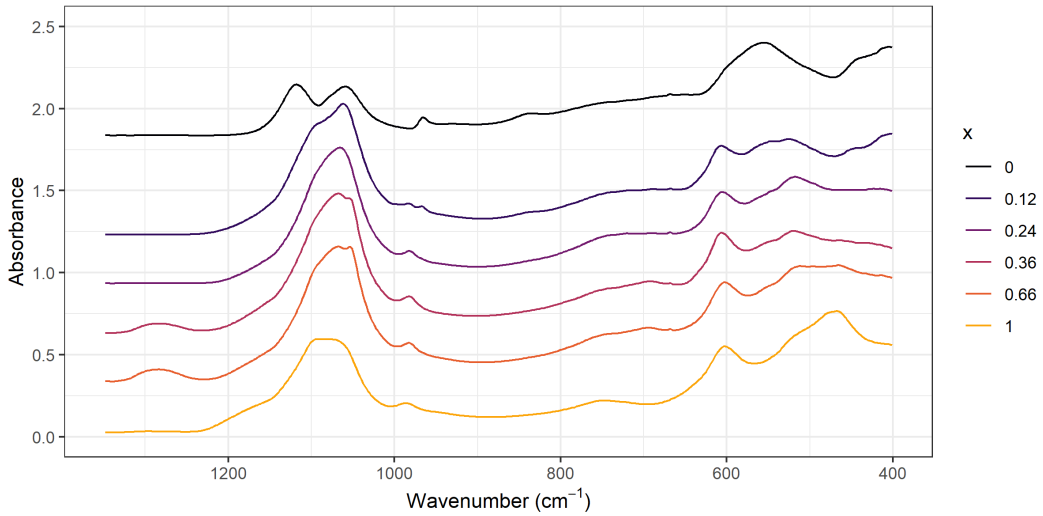

Figure S6: Infrared spectra for the R = 1.5 solid after various x addition of $S_2O_8^{2-}$

Figure S6 gathers the IR spectra of the R = 1.5 solids after various x. It is interesting to note that on the

x = 0 spectrum, one can observe two main bands in the region for the ν_3 vibration of sulfate (1059 and 1119 cm^{-1}). This split is similar as the one reported by Fan *et al* [3] for $Mn_5(OH)_8SO_4$ and can be explained by a anisotropic environment around the sulfate but may be also due to the presence of two different environments for the sulfate [4]. This split disappears at higher x value and only one band at 1067 cm^{-1} is observed. At x = 1, the sulfate band can be attributed to sulfate associated to sodium in adventitious Na_2SO_4.

Beside this feature, another peak is changed during oxidation: an additional non attributed absorption band at 966 cm^{-1} disappears as x increases and a new band at 982 cm^{-1} appears. On the x = 0.12 spectrum, both can be seen, which confirm the fact that this solid is a mixture of two different products, as shown on Figure S6.

For lower wavenumbers, a strict attribution of the peaks is not straightforward. The band at 555 cm^{-1} is in line with previous work by Fan *et al* as well as Salah *et al* observing a large band slightly above 500 cm^{-1} [3, 5] for $Mn_5(OH)_8SO_4$ and $Mn_2(OH)_2SO_4$ respectively. Then, the evolution of those peaks for increasing x shows the transformation of the solid during oxidation.

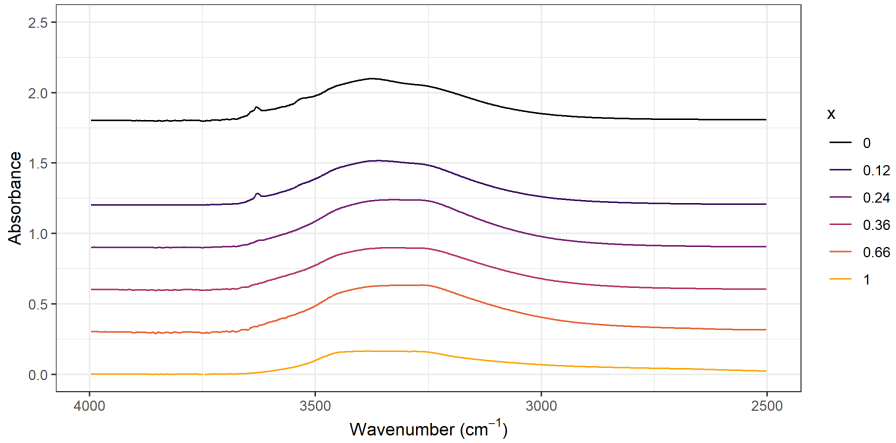

Figure S7: OH stretching region of the Mn-LDH

The same spectra but for higher wavenumbers on Figure S7 show the evolution of the O-H stretching during oxidation and the decrease of the absorbance in this region for the x = 1 product.

3.4 XPS characterization

Surface properties of Mn-LDH were examined by XPS. Overview XPS spectra (not shown) show core-level photoelectron peaks around 169 eV (S2p), 285 eV (C1s), 532 eV (O1s), 641 eV ($Mn2p_3/2$), 652 eV ($Mn2p_1/2$) and 1071 eV (Na1s). The C1s peak should be attributed to atmospheric hydrocarbon contamination of the Mn-LDH surface.

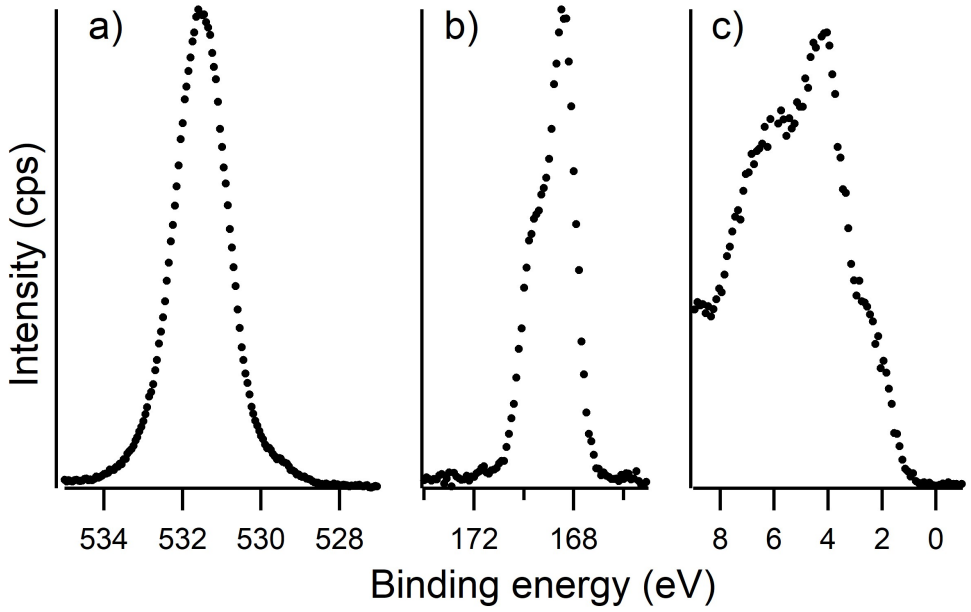

Figure S8: XPS of the solids for R = 1.5 and x = 0.24 ratios (black dots) in the $S2p_{3/2}$ region (a), O1s region (b) and valence band (c).

S2p high-resolution spectrum (Figure S8 a) presents $S2p_{3/2}$ and $S2p_{1/2}$ (168.5 and 169.7 eV) components corresponding to sulfur in sulfate form. This signal may be attributed to sulfate in the interlayer space as well as from sulfate associated to sodium in adventitious Na_2SO_4.

The O1s spectra (figure S8 b) presents a maximum at 531.4 eV essentially attributed to hydroxyl species.

The valence band (VB) spectrum (figure S8 c) is dominated by a peak at 4.3 eV with shoulders at 2.4 and 6.4 eV. The locations of these features are close to the ones reported for MnO or Mn_2O_3 [6, 7, 8]. The top of the VB (at 50% of the low binding energy shoulder) is located around 1.7 eV with respect to Fermi edge. Considering Mn ions in high-spin octahedral environment, photoemission signal at low binding energy might be due to 3d electron removal from e_g and t_{2g}. The predict intensity ratio 3/2 for Mn^{2+} ion is in the order of magnitude to what is observed for 2.4 and 4.3 eV features. Nevertheless, overlap with Mn^{III} contribution complicates the picture and further insight into VB interpretation would necessitate simulations [9] that are far beyond the scope of this work.

3.5 Thermogravimetric properties

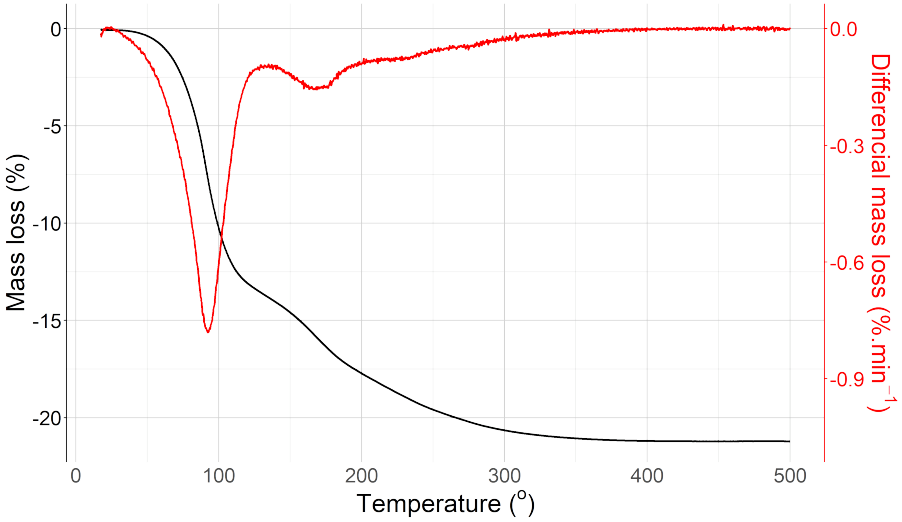

Figure S9: Thermogravimetric analysis of the LDH compound, black is the mass loss, red the differentiate mass loss

3.6 Magnetic properties

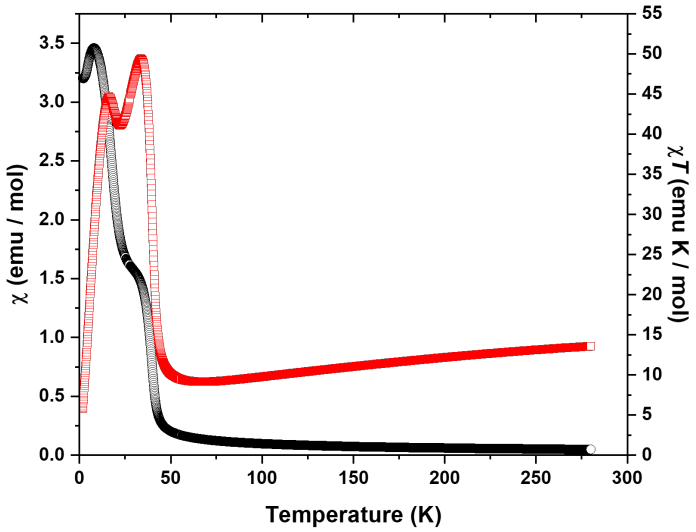

Figure S10: χ = f(T) (black circles) and χT = f(T) (red squares) for compound LDH-Mn, under a dc field of 0.5 T.

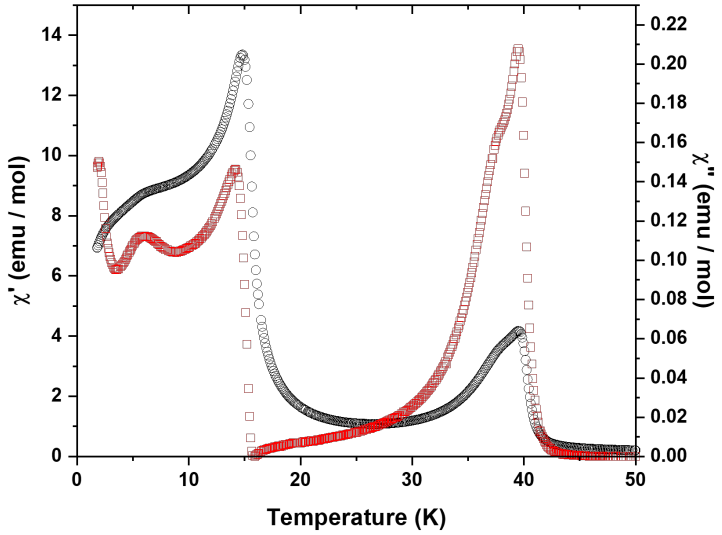

Figure S11: In-phase (χ' (black circles)) and out-of-phase (χ" (red squares)) as a function of temperature (zero static dc field, 2 Oe oscillating field at a frequency of 95 Hz).

4 Thermodynamic considerations

4.1 Estimation of the standard Gibbs free energy of formation of the Mn^{II}-Mn^{III} LDH

A value E_h^0(MnO(OH)/Mn-LDH) = + 1.117 V/SHE was computed from equation 2 by using the experimental E_h/ESH value (+380 mV) corrected from the E_h/SCE electrode (KCl concentration: 3 mol.L^{-1}, E(SCE) = 210 mV/ESH and pH value (8.2).

The corresponding half reaction and Nernst equation are given in equation 1 and 2, respectively:

$$[Mn_4^{II}Mn_2^{III}(OH)_{12}][SO_4^{2-}]_{(s)} + 6H_2O_{(l)} \rightleftharpoons 6MnO(OH)_{(s)} + {SO_4^{2-}}_{(aq)} + 6{H_3O^+}_{(aq)} + 4e^- \quad (1)$$

$$E_h(MnO(OH)_{(s)}/\text{Mn-LDH}_{(s)}) = E_h^0(MnO(OH)_{(s)}/\text{Mn-LDH}_{(s)}) - \frac{RT}{4F}\log_{10}[a({SO_4^{2-}}_{(aq)})] + \frac{6RT}{4F}pH \quad (2)$$

In a first approximation the activity $a(SO_4)$ was assumed to be equal to the concentration of sulfate species. This concentration was estimated to be about 0.35 mol.L^{-1} at the middle of plateau B, a value corresponding to the difference between the initial concentration of SO_4^{2-} in solution (0.4 mol.L^{-1}) and the quantity of sulfate incorporated into GRSO4 (about 0.05 mol.L^{-1}). Taking into account the activity coefficient of sulfate species as performed in other works [10] will have only a minor influence on the computed values of E_h^0. The standard Gibbs energy of formation of the Mn-LDH was estimated by using equation 3:

$$E_h^0(MnO(OH)_{(s)}/\text{Mn-LDH}_{(s)}) = \frac{6\Delta_f G^0(MnO(OH)_{(s)}) + \Delta_f G^0({SO_4^{2-}}_{(aq)}) - \Delta_f G^0(\text{Mn-LDH}_{(s)})}{4F} \quad (3)$$

with F = 96 485 C.mol^{-1} the Faraday constant.

Species	$\Delta_f G^0$(kJ.mol^{-1})	Reference
H_2O (l)	-237.19	[11]
$SO_4{}^{2-}$ (aq)	-744.56	[11]
$NO_3{}^-$ (aq)	-110.58	[12]
$NH_4{}^+$ (aq)	-79.5	[12]
NH_3 (aq)	-26.6	[11]
Fe^{2+} (aq)	-84.93	[12]
$Fe(OH)_2$ (s)	-483.55	[12]
$Fe^{II}{}_4Fe^{III}{}_2(OH)_{12}SO_4$ (s)	-3790	[10]
FeO(OH) (s)	-469.03	[12]
Mn^{2+} (aq)	-227.61	[12]
$Mn(OH)_2$ (s)	-614.63	[12]
$Mn_4{}^{II}Mn_2{}^{III}(OH)_{12}SO_4$ (s)	[-4519, -4436]	This work
γ-MnO(OH) (s)	-557.2	[13]
β-MnO(OH) (s)	-543.4	[13]

Table S3: Reference Standard Gibbs free energy of formation $\Delta_f G^0$(kJ.mol^{-1}). The standard Gibbs energy of formation of groutite $\alpha - MnO(OH)_{(s)}$ (no data available) was supposed to be close from feitknechtite $\beta - MnO(OH)_{(s)}$ Indeed, both compounds were reported to be less stable than manganite $\gamma - MnO(OH)_{(s)}$ [14] with corresponding higher $\Delta_f G^0$ values.

4.2 Pourbaix Diagrams

The electrochemical equilibria were considered at room temperature (T = 298 K) and the activities of the soluble species was fixed at 10^{-2}. Mn_0 (s), Mn^{2+} (aq), $Mn(OH)_2$ (s), Mn-LDH (s) and γ-MnOOH (s) species were considered for the Mn Pourbaix diagram (Main text Figure 7A). Basic salts with Mn mentioned in this study were not added as their thermodynamic properties are little known. Similarly, Fe_0 (s), Fe^{2+} (aq), $Fe(OH)_2$ (s), Fe-LDH (s) and γ-FeOOH (s) species were considered for the drawing the Fe Pourbaix diagram (Main text Figure 7B). The stability domains of Mn^{2+} (aq) and Mn-LDH (s) are much broader than those of Fe^{2+} (aq) and Fe-LDH (s). The relative stability of the Mn-LDH in comparison to Fe-LDH can also be illustrated by studying their potential reactivity towards nitrate species. For this purpose, the following $NO_3{}^-$ (aq) reduction reactions were considered:

$$2NO^-_{3(aq)} + 10e^- + 12H_3O^+_{(aq)} = N_{2(g)} + 18H_2O_{(l)} \quad (4)$$

$$NO^-_{3(aq)} + 8e^- + 10H_3O^+_{(aq)} = NH^+_{4(aq)} + 13H_2O_{(l)} \quad (5)$$

$$NO^-_{3(aq)} + 8e^- + 9H_3O^+_{(aq)} = NH_{3(aq)} + 12H_2O_{(l)} \quad (6)$$

The corresponding Nernst equations computed for T = 298 K are the following :

$$E_h(NO^-_{3(aq)}/N_{2(g)}) = E^0_h(NO^-_{3(aq)}/N_{2(g)}) + \frac{RT}{10F}\log_{10}[\frac{a(NO^-_{3(aq)})^2}{a(N_{2(g)})}] - \frac{12RT}{10F}pH \quad (7)$$

For equation 4 with $E_h^0(NO_{3(aq)}^-/N_{2(g)}) = 1.24$ V/SHE and $a(N_{2(g)}) = 1$, $a(NO_{3(aq)}^-) = 0.01$.

$$E_h(NO_{3(aq)}^-/NH_{4(aq)}^+) = E_h^0(NO_{3(aq)}^-/NH_{4(aq)}^+) + \frac{RT}{8F}\log_{10}[\frac{a(NO_{3(aq)}^-)}{a(NH_{4(aq)}^+)}] - \frac{10RT}{8F}pH \quad (8)$$

For equation 5 with $E_h^0(NO_{3(aq)}^-/NH_{4(aq)^+}) = 0.88$ V/SHE and $a(NO_{3(aq)}^-) = a(NH_{4(aq)}^+) = 0.01$.

$$E_h(NO_{3(aq)}^-/NH_{3(aq)}) = E_h^0(NO_{3(aq)}^-/NH_{3(aq)}) + \frac{RT}{8F}\log_{10}[\frac{a(NO_{3(aq)}^-)}{a(NH_{3(aq)})}] - \frac{9RT}{8F}pH \quad (9)$$

For equation 6 with $E_h^0(NO_{3(aq)}^-/NH_{3(aq)}) = 0.81$ V/SHE and $a(NO_{3(aq)}^-) = a(NH_{4(aq)}^+) = 0.01$.

Equations 7, 8 and 9 were superimposed on the Pourbaix diagrams and correspond to lines 8, 9a and 9b, respectively (Main text Figure 6 A and B).

References

[1] Damien Cornu, Romain Coustel, Pierrick Durand, Cédric Carteret, and Christian Ruby. How can pH drop while adding NaOH? Formation and transformation of Mn4(OH)64. *Journal of Solid State Chemistry*, page 122631, October 2021.

[2] R. Scholder and H. Kyri. Über die Oxydation von Mangan(II)-hydroxyd mit Sauerstoff in konzentrierten Laugen. *Zeitschrift für anorganische und allgemeine Chemie*, 270(1-4):56–68, 1952.

[3] Yong Fan, Guang Hua Li, Lei Yang, Zhi Ming Zhang, Yan Chen, Tian You Song, and Shou Hua Feng. Synthesis, Crystal Structure, and Magnetic Properties of a Three-Dimensional Hydroxide Sulfate: Mn5(OH)8SO4. *European Journal of Inorganic Chemistry*, 2005(16):3359–3364, 2005.

[4] Melissa D. Lane. Mid-infrared emission spectroscopy of sulfate and sulfate-bearing minerals. *American Mineralogist*, 92(1):1–18, January 2007.

[5] Mohsen Ben Salah, Serge Vilminot, Tahar Mhiri, and Mohamedally Kurmoo. Synthesis, Crystal Structure, and Magnetic Properties of Mn2(OH)2SO4: A Novel Layered Hydroxide. *European Journal of Inorganic Chemistry*, 2004(11):2272–2276, 2004.

[6] J. van Elp, R. H. Potze, H. Eskes, R. Berger, and G. A. Sawatzky. Electronic structure of MnO. *Physical Review B*, 44(4):1530–1537, July 1991.

[7] Asish K. Kundu, Sukanta Barman, and Krishnakumar S. R. Menon. Effects of film thickness and magnetism on the electronic structure of MnO films. *Physical Review B*, 96(19):195116, November 2017.

[8] Ahmad Ali Audi and Peter M. A. Sherwood. Valence-band x-ray photoelectron spectroscopic studies of manganese and its oxides interpreted by cluster and band structure calculations. *Surface and Interface Analysis*, 33(3):274–282, 2002.

[9] C. Franchini, R. Podloucky, J. Paier, M. Marsman, and G. Kresse. Ground-state properties of multivalent manganese oxides: Density functional and hybrid density functional calculations. *Physical Review B*, 75(19):195128, May 2007.

[10] P. Refait, C. Bon, L. Simon, G. Bourrie, F. Trolard, J. Bessiere, and J. M. R. Genin. Chemical composition and Gibbs standard free energy of formation of Fe(II)-Fe(III) hydroxysulphate green rust and Fe(II) hydroxide. *Clay Minerals*, 34(3):499–510, September 1999.

[11] A. J. Bard, R. Parsons, and J. Jordan. Standard potentials in aqueous solution. January 1985.

[12] J Van Muylder and M Pourbaix. Atlas d'équilibres électrochimiques à 25 C. *Gauthier-Villars & Cie, Paris*, page 378, 1963.

[13] Owen Bricker. Some stability relations in the system Mn-O2-H2O at 25 and one atmosphere total pressure. *American Mineralogist*, 50(9):1296–1354, September 1965.

[14] John D. Hem and Carol J. Lind. Nonequilibrium models for predicting forms of precipitated manganese oxides. *Geochimica et Cosmochimica Acta*, 47(11):2037–2046, November 1983.